Available online at www.sciencedirect.com
SCIENCE DIRECT®
Journal of Magnetism and Magnetic Materials 272–276 (2004) 1706–1711
Journal of magnetism and magnetic materials
www.elsevier.com/locate/jmmm

Magnetization reversal by injection and transfer of spin: experiments and theory

A. Fert[a,e,*], V. Cros[a], J.-M. George[a], J. Grollier[a], H. Jaffrès[a], A. Hamzic[a,b], A. Vaurès[a], G. Faini[c], J. Ben Youssef[d], H. Le Gall[d]

[a] *Unité Mixte de Physique CNRS/THALES, Thales Research Technology, Domaine de Corbeville, Orsay 91404, France*
[b] *Faculty of Science, University of Zagreb, Croatia*
[c] *Laboratoire de Photonique et de Nanostructures, Route de Nozay, Marcoussis 91460, France*
[d] *Laboratoire de Magnétisme de Bretagne, Brest 29285, France*
[e] *Université Paris-Sud, Orsay 91405, France*

Abstract

Reversing the magnetization of a ferromagnet by spin transfer from a current, rather than by applying a magnetic field, is the central idea of an extensive current research. After a review of our experiments of current-induced magnetization reversal in Co/Cu/Co trilayered pillars, we present the model we have worked out for the calculation of the current-induced torque and the interpretation of the experiments.

PACS: 75.60.Jk; 75.70.Cn; 73.40.−c

Keywords: Spintronics; Spin transport; Spin transfer

1. Introduction

The concept of magnetization reversal by spin transfer from a spin-polarized current was introduced in 1996 by Slonczewski [1]. Similar ideas of spin transfer had also appeared in the earlier work of Berger [2] on current-induced domain wall motion. Convincing experiments of magnetization reversal by spin transfer on pillar-shaped multilayers [3–6], nanowires [7] or nanocontacts [8] have been recently performed and several theoretical approaches, extending the initial theory, have also been developed [9–19]. From the application point of view, magnetization reversal by spin transfer can be of great interest to switch spintronic devices (MRAM for example), especially if the required current density—presently around 10^7 A/cm^2—can be reduced by approximately an order of magnitude.

We present a summary of our experiments on Co/Cu/Co pillars, describe a calculation model for the critical currents as a function of—mainly—CPP-GMR data and we discuss its application to experiments.

2. Experiments

We present experiments on pillar-shaped Co1(2.5 nm)/Cu(10 nm)/Co2(15 nm) trilayers. The submicronic (200×600 nm^2) pillars are fabricated by e-beam lithography [5]. The CCP-GMR of the trilayer is used to detect the changes of the magnetic configuration (the difference between the resistances of the P and AP configurations is about 1 mΩ). For all the experiments, we describe, the initial magnetic configuration is a parallel (P) one, with the magnetic moments of the Co layers along the positive direction of an axis parallel to the long side of the rectangular pillar. A field H_{appl} is

*Corresponding author. Unité Mixte de Physique CNRS/THALES, Thales Research Technology, Domaine de Corbeville, Orsay 91404, France. Tel.: +33-1-69-33-91-05; fax: +33-1-69-33-07-40.
E-mail address: albert.fert@thalesgroup.com (A. Fert).

0304-8853/$ - see front matter © 2003 Elsevier B.V. All rights reserved.
doi:10.1016/j.jmmm.2003.12.1351

applied along the positive direction of this axis (thus stabilizing this initial P magnetic configuration). We record the variation of the resistance (R) as the current I is increased or decreased (positive I means electrons going from the thick Co layer to the thin one). The results we report here are obtained at 30 K (the critical currents are smaller at room temperature).

In Fig. 1(a), we present a typical variation of the resistance R as a function of the current, for $H_{appl} = 0$ and +125 Oe. Starting from a P configuration at $I = 0$ and increasing the current to positive values, we observe only a small progressive and reversible increase of the resistance, which can be ascribed to Joule heating (this has also been seen in all other experiments on pillars [3–6] when the current density reaches the range of 10^7 A/cm^2). In contrast, when the current is negative and at a critical value $I_C^{P\to AP}$, there is an irreversible jump of the resistance ($\Delta R \approx 1$ mΩ), which corresponds to a transition from the P to the AP configuration (reversal of the magnetic moment of the thin Co layer). The trilayer then remains in this high resistance state (the $R_{AP}(I)$ curve) until the current is reversed and increased to the critical value $I_C^{AP\to P}$, where the resistance drops back to the $R_P(I)$ curve. This type of hysteretic $R(I)$ cycle is characteristic of the magnetization reversal by spin injection in *regime A*.

For $H_{appl} = 0$, $I_C^{P\to AP} \cong -15$ mA (current density $j_C^{P\to AP} \cong -1.25 \times 10^7$ A/cm^2) and $I_C^{AP\to P} \cong +14$ mA ($j_C^{AP\to P} \cong +1.17 \times 10^7$ A/cm^2). A positive field, which stabilizes the P configuration, shifts slightly the critical currents; $|I_C^{P\to AP}|$ increases and $I_C^{AP\to P}$ decreases (note that the relatively larger shift of $I_C^{AP\to P}$ at 125 Oe in Fig. 1(a) is specific to the approach to the crossover to *regime B* at about 150 Oe).

The $R(I)$ curve for $H_{appl} = +500$ Oe, shown in Fig. 1(b), illustrates the different behavior when the applied field is higher (*regime B*). Starting from $I = 0$ in a P configuration (on the $R_P(I)$ curve), a large enough negative current still induces a transition from P to AP, but now this transition is *progressive* and *reversible*. The $R(I)$ curve departs from the $R_P(I)$ curve at $I_{start}^{P\to AP} \cong -25$ mA ($j_{start}^{P\to AP} \cong -2.08 \times 10^7$ A/cm^2) and catches up the $R_{AP}(I)$ curve only at $I_{end}^{P\to AP} \cong -45$ mA ($j_{end}^{P\to AP} \cong -3.75 \times 10^7$ A/cm^2). On the way back, reversibly, $R(I)$ departs from $R_{AP}(I)$ at $I_{start}^{AP\to P} = I_{end}^{P\to AP} \cong -45$ mA and reaches finally $R_P(I)$ at $I_{end}^{AP\to P} = I_{start}^{P\to AP} \cong -25$ mA. At higher field, the transition is similarly progressive and reversible, but occurs in a higher negative current range. Finally, for very large applied field ($H_{appl} = 5000$ Oe), the transition is out of our experimental current range, and the recorded curve is simply $R_P(I)$.

The experimental results presented above can be summarized by the diagram in Fig. 2. This type of diagram is obtained [18] by introducing the current-induced torque into a Landau–Lifshitz–Gilbert (LLG) motion equation to study the stability/instability of the moment of the magnetic thin layer (the moment of the thick layer supposed being pinned). The P configuration is stable above *line* 1 and unstable below. The AP configuration is stable below *line* 2 and unstable above.

Regime A corresponds to H_{appl} smaller than the field at which *line* 2 crosses *line* 1. In this regime, there is an overlap between the stability regions of P and AP. Starting from a P configuration at zero current and moving downward on a vertical line, the P configuration becomes unstable at the negative current $I_C^{P\to AP}$ corresponding to the crossing point with *line* 1. As this point in the stability region of the AP configuration, the unstable P configuration can switch directly to the stable AP configuration. On the way back, the AP configuration remains stable until the crossing point with *line* 2 at $I_C^{AP\to P}$ (positive), where it can switch directly to a stable P configuration. This accounts for the direct transitions and hysteretic behavior of *regime A* in Fig. 1(a). Note the bistability can only predict the possibility of direct transitions but does not demonstrate that the transitions are necessarily direct.

In *regime B*, for H_{appl} above the crossing point of *lines* 1 and 2, none of the P and AP configurations is stable in

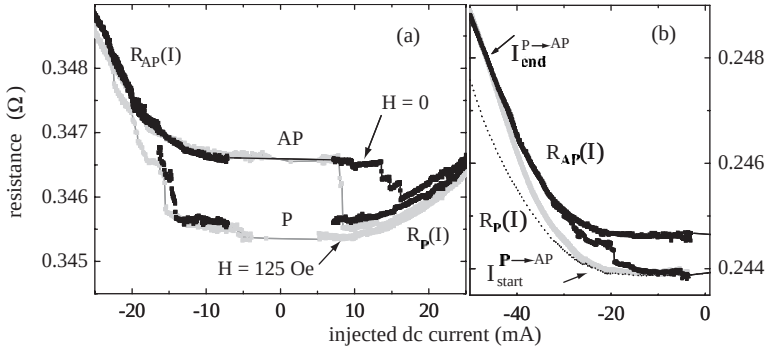

Fig. 1. Resistance vs. dc current: (a) sample 1 for $H_{appl} = 0$ (black) and $H_{appl} = 125$ Oe (gray); (b) sample 2 for $H_{appl} = 0$ (black), $H_{appl} = +500$ Oe (gray) and $H_{appl} = +5000$ Oe (dotted line).

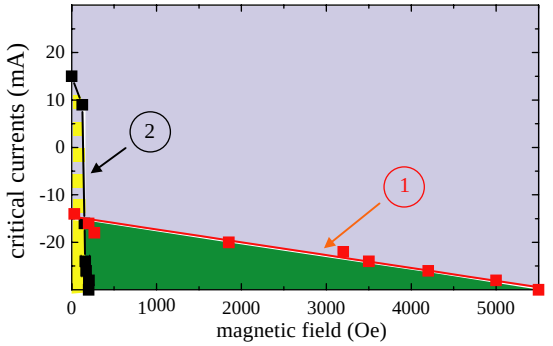

Fig. 2. Instability lines of the P and AP configurations (sample 1). The P configuration is stable above *line* 1 and unstable below. The AP one is stable below *line* 2 and unstable above. At low field (*regime A*), the stability zones of P (blue) and AP (yellow) overlap between *lines* 1 and 2 (stripes). At high field (*regime B*), there is a zone (green) between *lines* 1 and 2 where none of the P and AP configurations is stable. Equations of *lines* 1 and 2 are derived from a LLG equation for uniaxial anisotropy H_{an} [18]. The magnetic field includes $H_{appl.}$ and, possibly, interlayer coupling fields. *lines* 1 and 2 cross at about H_{an}.

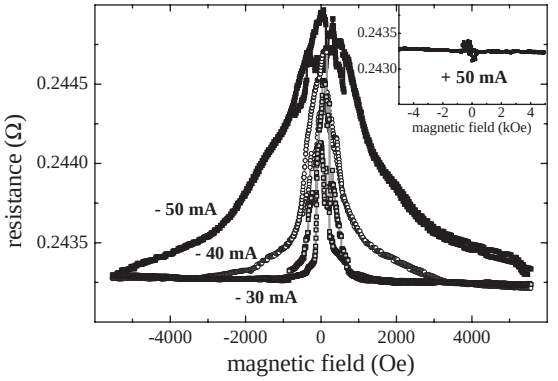

Fig. 3. Resistance vs. applied magnetic field in sample 2 for $I = -50$, -40, and -30 mA. For clarity, the curves have been shifted vertically to have the same high field baseline. inset: $R(H)$ for $I = +50$ mA.

the region between *lines* 1 and 2. Going down along a vertical line, the P configuration becomes unstable at the crossing point with *line* 1 ($I_{start}^{P\to AP}$) and the system departs from this configuration. But the AP configuration is still unstable at this current and can be reached only at the crossing point with *line* 2 ($I_{end}^{P\to AP}$). On the way back, reversibly, the AP configuration becomes unstable at the crossing point with *line* 2 ($I_{start}^{AP\to P} = I_{end}^{P\to AP}$), but a stable P configuration is reached only at the crossing point with *line* 1 ($I_{end}^{AP\to P} = I_{start}^{P\to AP}$). This accounts for the behavior of Fig. 1(b). The state of the system during the progressive transition between P and AP can be described as a state of maintained precession.

The critical lines of the diagram of Fig. 2 can also be derived from the variation of R along a horizontal line, for example from the $R(H_{appl})$ curves of Fig. 3 for sample 2. The $R(H_{appl})$ curve for $I = +50$ mA is flat, i.e. there is no GMR. This is because, along an horizontal line in the upper part of the diagram of Fig. 2, the P configuration is always stable. For negative current, on the other hand, the $R(H_{appl})$ curves mimic the GMR curves of an antiferromagnetically coupled trilayer, in which the antiferromagnetic coupling would increase when the current becomes more negative. This can be expected from the diagram of Fig. 2. For example, starting from high field at $I = -50$ mA, the upturn from the baseline at about $H_{appl} = +5600$ Oe indicates the beginning of the progressive transition from P to AP at the crossing point with *line* 1. As H_{appl} is decreased further, the progressive (and reversible) increase of R reflects the progressive crossover from P to AP on a horizontal line between *line* 1 at 5600 Oe and *line* 2 at a field in the range 100–200 Oe. When the moment of the thick Co layer is reversed in a small negative field, the P configuration being unstable and the AP stable in this region of the diagram, the moment of the thin layer is also reversed to restore the AP configuration, so that R is practically not affected by the coupled reversal of both layers.

We conclude that the main features of the experimental results fit into the frame of the diagram of Fig. 2. In Section 4, we discuss more quantitatively the influence of parameters such as layer thicknesses, spin diffusion length, etc. The final remark of this section is that the phase diagram of Fig. 2 comes from an oversimplified model assuming that the only current-induced excitations are precessions of a global magnetization vector due to transverse spin transfer. Several types of additional effects can be expected from non-uniform precessions, or, more generally, from other modes of current-induced excitations. For example, excitation of magnons plays an important role in point contact experiments in which spin waves can be radiated from the point contact into an extended layer [8,10]. The interplay between the coherent precession of the zero temperature model [18] and thermal or current-induced fluctuations is also necessary to explain the decrease of the critical currents with temperature and the telegraphic noise observed near the transitions. Other effects [6] are also expected from exchange or dipolar interlayer couplings which can play the same role as the applied field in Fig. 2.

3. Theoretical model

The magnetization of a magnetic layer can be reversed by spin transfer if the spin polarization of the injected

current and the magnetization of the layer are non-collinear. In a multilayered structure this requires a non-collinear configuration of the magnetizations of the different layers. The transfer from an obliquely polarized spin current running into a magnetic layer is associated with the alignment of the polarization of the current inside the layer along the magnetization axis. If the current-layer interaction is spin conserving (exchange-like), this implies that the transverse component of the spin current is absorbed and transferred to the layer. This is the spin transfer concept introduced by Slonczewski [1]. The contribution of this transfer to the motion equation of the total spin S of the layer is written as

$$(d\mathbf{S}/dt)_j = \text{absorbed transv. spin current} \quad (1)$$

or, in other words, a torque equal to the absorbed spin current multiplied by $\hbar$ is acting on the magnetic moment of the layer.

Several mechanisms contribute to the transfer of the transverse component of a spin current running into a magnetic layer [12]. First, due to the spin dependence of the reflection/transmission process at the interface with a ferromagnet, the transverse component is reduced and rotated in the transmitted spin current. What remains of transverse component then disappears (is transferred) by incoherent precession of the electron spins in the exchange field of the ferromagnet. Ab initio calculations [12] show that, for a metal like Co, the transverse spin current is almost completely absorbed at a distance of the order of 1 nm from the interface. In these conditions, the spin transfer is a quasi-interfacial effect and, in our calculation, is expressed by interface boundary conditions (in the same way as interface resistances are introduced in boundary conditions for the theory of CPP-GMR [20]). On the other hand, the longitudinal component of the spin current in the magnetic layers and all its components in the non-magnetic layers vary at the much longer scale of the spin diffusion length l_{sf} (60 nm in Co, about 1 μm in Cu). They can be calculated by solving diffusive transport equations for the entire structure, as in the theory of the CPP-GMR. An essential point is that, for a non-collinear configuration with different orientations of the longitudinal axes in different layers, the longitudinal and transverse components of the spin current are inter-twined from one layer to the next one, so that a global solution for both the longitudinal and transverse component and for the entire structure is required.

The calculation of our model can be summarized as follows. We consider a $N_L/F_1/N/F_2/N_R$ structure, where F_1 (thin) and F_2 (thick) are ferromagnetic layers separated by a t_N thick non-magnetic layer N. N_L and N_R are two semi-infinite non-magnetic layers (leads). For simplicity we assume that F_1 and F_2 (N, N_L and N_R) are made of the same ferromagnetic (non-magnetic) material. The current is along the x-axis perpendicular to the layers. $\hat{m}(x)$ and $\hat{j}(x)$ are the 2×2 matrices representing, respectively, the spin accumulation and the current density:

$$\hat{j}(x) = \frac{j_e}{e}\hat{I} + j_{m,x}(x)\hat{\sigma}_x + j_{m,y}(x)\hat{\sigma}_y + j_{m,z}(x)\hat{\sigma}_z,$$

$$\hat{m}(x) = m_x(x)\hat{\sigma}_x + m_y(x)\hat{\sigma}_y + m_z(x)\hat{\sigma}_z, \quad (2)$$

where $\hat{\sigma}_x$, $\hat{\sigma}_y$ and $\hat{\sigma}_z$ are the three Pauli matrices and $\hat{I}$ is the unitary matrix. Spin accumulation and current are defined as in Ref. [13]. If we call z_i the local spin polarization axis ($z_i = z_1$ in F_1, and z_2 in F_2), m_{z_i} (j_{m,z_i}) is the longitudinal component of the spin accumulation vector $\mathbf{m}$ (spin current vector $\mathbf{j}_m$), m_{x_i} and m_{y_i} (j_{m,x_i} and j_{m,y_i}) are the transverse components of $\mathbf{m}$ ($\mathbf{j}_m$).

To derive the critical currents for the instability of the P and AP configurations, we need only to calculate the current-induced torque in the simple limit where the angle between the magnetizations of the magnetic layers is small or close to π (θ or $\pi-\theta$, with θ small). The first step, before introducing the small angle θ, is the calculation of the longitudinal spin current j_{mz} and spin accumulation m_z in a collinear configuration ($\theta = 0$). This is done by using the standard diffusive transport equations of the theory of the CPP-GMR with parameters (spin-dependent interface resistances, interface spin memory loss coefficient, spin diffusion lengths, etc.) derived from CPP-GMR experiments [21,22]. An example of the result for the P configuration of a Co/Cu/Co trilayer is shown at the top left of Fig. 4. In the bottom part of Fig. 4, we represent the situation when a small deviation θ from the parallel collinear configuration above is introduced. The spin accumulation in the Cu spacer layer is a constant vector $\mathbf{m}$ (as, generally, $t_{Cu} \ll l_{sf}^{Cu}$). With respect to the collinear configuration, the amplitude of $\mathbf{m}$ has changed by a quantity of the first order in θ (we omit this part of the calculation). However, to calculate the torque at first order in θ, we can neglect this change and assume $|\mathbf{m}| = m_{Cu}^{P}$, where m_{Cu}^{P} is the spin accumulation m_z in Cu for the P collinear configuration. On the other hand, $\mathbf{m}$ cannot be parallel to both z_1 and z_2, and its orientation in the frame of the thin layer is characterized by the unknown angles θ_m (of the order of θ) and χ. These angles will be determined later by self-consistency conditions for the whole structure. The key point, explaining the injection of a large transverse spin current into the thin magnetic layer, is the discontinuity of transverse spin accumulation between the two sides of the interface between Cu and Co1, $|\mathbf{m}| = \theta_m m_{Cu}^{P}$ in Cu and $|\mathbf{m}| = 0$ in Co1. This is equivalent to a huge gradient of spin accumulation and generates a large transverse spin diffusion current running into the interface where it is absorbed or reflected. A straightforward angular integration, illustrated at the top right of Fig. 4, gives for the incoming

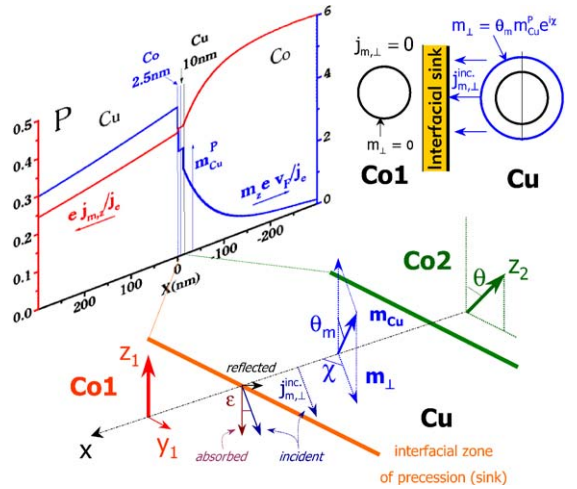

Fig. 4. Top left: profile of the spin current $\mathbf{j}_{m,z}$ and spin accumulation $\mathbf{m}_z$ calculated from diffusive CPP-transport equations and CPP-GMR data for a (Cu/Co1 2.5 nm/Cu 10 nm/Co2 ∞) structure in a parallel collinear configuration with an electron current (j_e) going to the left. Bottom: for a small angle θ between the polarization axes z_1 (vertical) and z_2 of the same structure, 3D sketch representing the spin accumulation $\mathbf{m}$ in the Cu layer ($|\mathbf{m}| = m^{\mathrm{P}}_{\mathrm{Cu}}$ of the collinear configuration), its transverse component $m_\perp$ and the transverse component of the induced spin currents diffusing to, reflected from and absorbed by the Co1 layer. The angles θ_m and χ_m characterize the orientation of the vector $\mathbf{m}$ in the frame of Co1. Top right: schematic illustrating the calculation of the transverse spin diffusion current generated by the transverse spin accumulation on the Cu side of the Co1/Cu interface.

transverse spin current:

$$j^{\mathrm{inc.}}_{m,\perp} = \tfrac{1}{4}\theta_m e^{i\chi} m^{\mathrm{P}}_{\mathrm{Cu}} v_{\mathrm{F}}, \tag{3}$$

where $j^{\mathrm{inc.}}_{m,\perp} = j^{\mathrm{inc.}}_{m,x} + \mathrm{i} j^{\mathrm{inc.}}_{m,y}$ and v_{F} is the Fermi velocity. Eq. (3) holds for a spacer thickness of the order of the mean free path or larger. A part of this incoming transverse spin current is reflected into Cu at the Cu/Co1 interface. The remaining part absorbed in the interfacial precession zone can be written as $j^{\mathrm{abs.}}_{m,\perp} = t e^{i\varepsilon} j^{\mathrm{inc.}}_{m,\perp}$, where the coefficient t and the rotation angle ε have been calculated [12] for a large number of interfaces. This leads to

$$j^{\mathrm{abs.}}_{m,\perp} = \tfrac{1}{4}\theta_m t e^{i(\chi+\varepsilon)} m^{\mathrm{P}}_{\mathrm{Cu}} v_{\mathrm{F}}. \tag{4}$$

Eq. (4) is equivalent to the transverse boundary conditions involving the mixing conductance in the circuit theory formalism [15]. The scale of the transverse spin current of Eq. (4) is the product $m^{\mathrm{P}}_{\mathrm{Cu}} v_{\mathrm{F}}$ (or $m^{\mathrm{AP}}_{\mathrm{Cu}} v_{\mathrm{F}}$ around the AP state), where $m^{\mathrm{P}}_{\mathrm{Cu}}$ is controlled by the spin relaxation in the system. $m^{\mathrm{P}}_{\mathrm{Cu}} v_{\mathrm{F}}$ is of the order of $(j_e/e)\langle l_{\mathrm{sf}}/\lambda\rangle$, where $\langle l_{\mathrm{sf}}/\lambda\rangle$ is a mean value of the ratio of the spin diffusion length (SDL) to the mean free path (MFP) in the structure (including the leads), and can be definitely larger than the charge current j_e/e.

The unknown angles θ_m and χ are calculated [16] by imposing a global cancellation of the transverse spin currents outgoing from or reflected into the spacer layer. In the case of a small deviation θ from the P configuration, for example, this leads to $\theta_m = \theta/2$ and $\chi = \pi/2$. Finally, from Eq. (1) and by including not only the term of Eq. (4) but also the contribution to the transverse spin current $\propto m^{\mathrm{P}}_{\mathrm{Co}}$ due to the diffusion from Co2 for thin Cu layers and additional contributions ($\propto j^{\mathrm{P}}_{m,\mathrm{Cu}}, j^{\mathrm{P}}_{m,\mathrm{Co}}$) from the spin accumulation gradient, we obtain the following expression of the torque $\mathbf{\Gamma}^{\mathrm{P}}$:"

$$\frac{\mathbf{\Gamma}^{\mathrm{P}}}{\hbar} = \left[\left(\frac{v_{\mathrm{F}} m^{\mathrm{P}}_{\mathrm{Cu}}}{8} + \frac{j^{\mathrm{P}}_{m,\mathrm{Cu}}}{2}\right)(1 - e^{-t_{\mathrm{Cu}}/\lambda_{\mathrm{Cu}}}) + \left(\frac{v_{\mathrm{F}} m^{\mathrm{P}}_{\mathrm{Co}}}{4} + j^{\mathrm{P}}_{m,\mathrm{Co}}\right) e^{-t_{\mathrm{Cu}}/\lambda_{\mathrm{Cu}}}\right] \times \mathbf{M}_1 \wedge (\mathbf{M}_1 \wedge \mathbf{M}_2) \tag{5}$$

with a similar expression for $\mathbf{\Gamma}^{\mathrm{AP}}$ ($\mathbf{M}_1$ and $\mathbf{M}_2$ are unit vectors along the magnetizations, $m^{\mathrm{P}}_{\mathrm{Co}}$ and $j^{\mathrm{P}}_{\mathrm{Co}}$ are the spin accumulation and current at the Cu/Co2 interface in the collinear configuration). As ab initio calculations have shown that, for most interfaces between classical magnetic and non-magnetic metals [12], t is always close to 1 and ε very small ($t \cong 0.92$ and ε smaller than 3×10^{-2} for Cu(1 1 1)/Co, for example), we have supposed $t = 1, \varepsilon = 0$ and kept only the term $\mathbf{M}_1 \wedge (\mathbf{M}_1 \wedge \mathbf{M}_2)$ in an expression of the form $[\cos(\varepsilon)\mathbf{M}_1 \wedge (\mathbf{M}_1 \wedge \mathbf{M}_2) + \sin(\varepsilon)\mathbf{M}_1 \wedge \mathbf{M}_2]$ (assuming $\varepsilon = 0$ is equivalent to neglecting the small imaginary parts of the mixing conductances in circuit theory [15]). A similar expression, with opposite sign, is obtained for $\mathbf{\Gamma}^{\mathrm{AP}}$.

The important feature in Eq. (5) is the relation of the torque at small angle to the spin accumulation $\mathbf{m}$ and spin current $\mathbf{j}_m$ calculated for the P and AP collinear configurations. We emphasize that, due to the relevant length scale of this calculation, the result for $\mathbf{\Gamma}$ involves the entire structure (including a length of the order of the SDL in the leads). The spin currents $j^{\mathrm{P(AP)}}_{m,\mathrm{Cu}}$ are only a fraction of the charge current j_e/e. In contrast the terms $v_{\mathrm{F}} m^{\mathrm{P(AP)}}$, reflecting the diffusion currents generated by the transverse spin accumulation discontinuities in a non-collinear system, are of the order of $(j_e/e)\langle l_{\mathrm{sf}}/\lambda\rangle$ and can be larger than j_e/e (a special case, however, is that of a P configuration of a symmetric structure, for which $m^{\mathrm{P}}_{\mathrm{Cu}} = 0$). Enhancing the spin accumulation and increasing its ratio to the current j_e is certainly the most promising way to reduce the critical current, for example with materials in which a higher spin accumulation splitting can be expected (magnetic semiconductors ?). This dependence on SDL and "amplification" is also taken into account in the model of Stiles and Zangwill [11,12] or Kovalev et al. [15], and in recent calculations of Slonczewski [10]. This "amplification" also turns out in the model of Shpiro et al. [14] for the opposite limit of

non-interfacial transfer. The main difference between the two limits is the equal importance of the terms $\mathbf{M}_1 \wedge (\mathbf{M}_1 \wedge \mathbf{M}_2)$ and $\mathbf{M}_1 \wedge \mathbf{M}_2$ in the torque of Shpiro et al. [14]. We will see below that the experimental critical line diagram of Fig. 2 indicates a largely predominant $\mathbf{M}_1 \wedge (\mathbf{M}_1 \wedge \mathbf{M}_2)$ torque term.

4. Discussion and conclusion

Our expression of the torque, Eq. (5), can be applied to the interpretation of the experimental results.

(a) If the torque of Eq. (5) is written as $\hbar S G^{P(AP)} j_e \times \mathbf{M}_1 \wedge (\mathbf{M}_1 \wedge \mathbf{M}_2)$, where S is the total spin of the layer, and, when the excitation can only be an uniform precession, the critical currents at zero field are expressed as [3,17,18]:

$$j_C^{P\to AP} = -\frac{\alpha\gamma_0}{G^P}(H_{an} + 2\pi M),$$
$$j_C^{AP\to P} = \frac{\alpha\gamma_0}{G^{AP}}(H_{an} + 2\pi M), \quad (6)$$

where α is the Gilbert coefficient, H_{an} is the anisotropy field and M the magnetization. By using experimental data (interface resistances, interface spin memory loss coefficient, SDL, etc.) from CPP-GMR experiments [21,22] to calculate the spin accumulation in the Co/Cu/Co trilayer and then $\mathbf{\Gamma}^{P(AP)}$ and $G^{P(AP)}$ from Eq. (5), we obtain a reasonable agreement with our experiments: $j_C^{P\to AP} = -2.8 \times 10^7$ A/cm^2 (exp.: -1.25×10^7A/cm^2) and $j_C^{AP\to P} = +1.05 \times 10^7$ A/cm^2 (exp.:$+1.17 \times 10^7$ A/cm^2).[1]

What can be also predicted for the critical currents is: (i) their proportionality to the thickness of the thin magnetic layer (this follows from the assumption of interfacial transfer and has been already observed [3]); (ii) their decrease as the thickness of the thick magnetic layer increases, with saturation at a minimum level when the thickness exceeds the SDL (60 nm in Co at low temperatures, for example); (iii) their increase (at the scale of the mean free path in the spacer) when the spacer thickness increases; (iv) their definite dependence on the SDL in the layers and leads.

(b) In finite applied field, a diagram of the type of Fig. 2, with a crossover between the two regimes around $H = H_{an}$, is expected for a torque of the form $\mathbf{M}_1 \wedge (\mathbf{M}_1 \wedge \mathbf{M}_2)$. The equations of the critical lines and a fit with experimental data has been presented elsewhere [18]. The diagram expected for a torque $\mathbf{M}_1 \wedge \mathbf{M}_2$ does not include a zone where both the P and AP configurations are unstable (*regime B* with progressive and reversible transition) and cannot be fitted with the experiments on Co/Cu/Co trilayers.

Although the spin transfer effect begins to be better understood, the possibility of reducing sufficiently the critical currents for practical applications is still a pending question. For conventional ferromagnetic metals (Co, etc.) and from numerical applications of the model of this paper [16], some reduction seems possible but probably by less than an order of magnitude. As we have pointed out, a stronger reduction might be obtained with other types of magnetic materials permitting higher spin accumulations. On the other hand, another type of spin transfer effect is the current-induced domain wall motion [2]. According to recent experimental results of domain wall motion with relatively small current densities [23], this should be also a promising way for current-induced switching.

[1] These values are slightly different from those of Ref. [18] where the interface spin memory loss is not taken into account in the calculation.

References

[1] J. Slonczewski, J. Magn. Magn. Mater. 159 (1996) L1.
[2] L. Berger, J. Appl. Phys. 71 (1992) 2721;
L. Berger, Phys. Rev. B 54 (1996) 9353.
[3] J.A. Katine, Phys. Rev. Lett. 84 (2000) 3149;
F.J. Albert, et al., Appl. Phys. Lett. 77 (2000) 3809.
[4] J.Z. Sun, et al., Appl. Phys. Lett. 81 (2002) 2202.
[5] J. Grollier, et al., Appl. Phys. Lett. 78 (2001) 3663.
[6] S. Urazdhin, et al. cond-mat/0303149.
[7] J.E. Wegrove, et al., Europhys. Lett. 45 (1999) 626.
[8] M. Tsoi, et al., Phys. Rev. Lett. 80 (1998) 4281.
[9] X. Waintal, et al., Phys. Rev. B 62 (2000) 12317.
[10] J. Slonczewski, J. Magn. Magn. Mater. 247 (2002) 324;
L. Berger, J. Appl. Phys. 91 (2002) 6795.
[11] M. Stiles, A. Zangwill, Phys. Rev. B 66 (2002) 01440.
[12] M. Stiles, A. Zangwill, J. Appl. Phys. 91 (2002) 6812.
[13] S. Zhang, P.M. Levy, A. Fert, Phys. Rev. Lett. 88 (2002) 236601.
[14] A. Shpiro, P.M. Levy, S. Zhang, Phys. Rev. B 67 (2003) 104430.
[15] K. Xia, et al., Phys. Rev. B 65 (2002) 220401;
A. Kovalev, et al., Phys. Rev. B 66 (2002) 224424.
[16] A. Fert, et al., to be published.
[17] J.Z. Sun, Phys. Rev. B 62 (2000) 570.
[18] J. Grollier, et al., Phys. Rev. B 67 (2003) 174402.
[19] J. Miltat, et al., J. Appl. Phys. 89 (2001) 6982.
[20] T. Valet, A. Fert, Phys. Rev. B 48 (1993) 7099.
[21] J. Bass, W.P. Pratt, J. Magn. Magn. Mater. 200 (1999) 274;
A. Fert, L. Piraux, J. Magn. Magn. Mater. 200 (1999) 338.
[22] W. Park, et al., Phys. Rev. B 62 (2000) 1178.
[23] J. Grollier, et al., Appl. Phys. Lett. 83 (2003) 509.